JACS
JOURNAL OF THE AMERICAN CHEMICAL SOCIETY

Article

pubs.acs.org/JACS

Temperature Dependent Reversible *p*−*n*−*p* Type Conduction Switching with Colossal Change in Thermopower of Semiconducting AgCuS

Satya N. Guin,[†] Jaysree Pan,[§] Arghya Bhowmik,[§] Dirtha Sanyal,[‡] Umesh V. Waghmare,[§] and Kanishka Biswas*[,†]

[†]New Chemistry Unit and [§]Theoretical Sciences Unit, Jawaharlal Nehru Centre for Advanced Scientific Research (JNCASR), Jakkur P.O., Bangalore 560064, India

[‡]Variable Energy Cyclotron Centre, 1/AF Bidhannagar, Kolkata 700064, India

Supporting Information

ABSTRACT: Semiconductors have been fundamental to various devices that are typically operated with electric field, such as transistors, memories, sensors, and resistive switches. There is growing interest in the development of novel inorganic materials for use in transistors and semiconductor switches, which can be operated with a temperature gradient. Here, we show that a crystalline semiconducting noble metal sulfide, AgCuS, exhibits a sharp temperature dependent reversible *p*−*n*−*p* type conduction switching, along with a colossal change in the thermopower (ΔS of ~1757 μV K^{-1}) at the superionic phase transition (T of ~364 K). In addition, its thermal conductivity is ultralow in 300−550 K range giving AgCuS the ability to maintain temperature gradients. We have developed fundamental understanding of the phase transition and *p*−*n*−*p* type conduction switching in AgCuS through temperature dependent synchrotron powder X-ray diffraction, heat capacity, Raman spectroscopy, and positron annihilation spectroscopy measurements. Using first-principles calculations, we show that this rare combination of properties originates from an effective decoupling of electrical conduction and phonon transport associated with electronic states of the rigid sulfur sublattice and soft vibrations of the disordered cation sublattices, respectively. Temperature dependent *p*−*n*−*p* type conduction switching makes AgCuS an ideal material for diode or transistor devices that operate reversibly on temperature or voltage changes near room temperature.

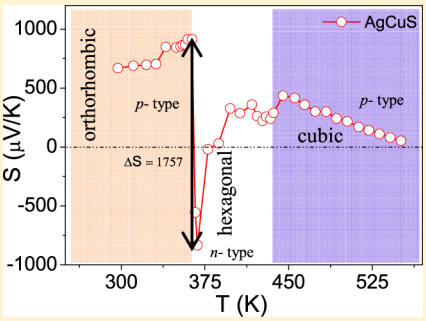

INTRODUCTION

Structural phase transformation is a common phenomenon in materials that is of fundamental interest to solid state inorganic chemistry.[1] Besides structural rearrangement, such a phase transformation can also involve changes in electronic or spin configurations, bringing in novel physical properties, such as superconductivity,[2] superionic conduction,[3,4] optical storage,[5] and giant magnetocaloric effect.[6] Switching of a material's property by external stimuli is interesting because of the fundamental science of bistability and nonlinearity, as well as of its possible technological applications.[7,8] Design and control of the changes in physical properties associated with a phase transition have been key to development of modern functional materials.[9] Among various inorganic materials, semiconductors have been versatile in their use in transistors, non volatile memory devices, electrochemical energy storage devices, resistive switching devices, thermoelectric energy conversion, and sensor applications.[10−14] Silver and copper chalcogenides, chalco-halides, and halides form a special class of semiconductors,[3,4,10] as they typically exhibit mixed ionic and electronic conduction in their superionic phases. These compounds are made of weakly coupled cationic and anionic substructures,[4,8,15] and undergo a transition to a superionic phase with changes in the substructure of mobile ions. Their electronic and phonon spectra can thus be modulated due to the sudden change in the ionic mobility or in the covalent interactions within the anionic substructure.[8,11,16,17] For example, $Ag_{10}Te_4Br_3$ is capable of switching its electrical conduction induced by a change of temperature and, hence, can be used as a switch.[10] The formation of *p*−*n* or *p*−*n*−*p* junctions can be induced in such mixed ionic-electronic conductors simply by altering external electrochemical potential or temperature gradients.[7,10,18] Silver and copper based chalcogenides are also recognized as good candidates for metal−insulator−metal type non volatile memory devices.[11,19]

Silver copper sulfide, AgCuS, is a polymorphous semiconductor that exhibits fascinating phase transitions as a function of temperature due to changes in the cationic mobilty.[20,21] Existence of four different polymorphs of AgCuS has been reported.[21] At room temperature, AgCuS crystallizes in the orthorhombic phase, β-AgCuS ($Cmc2_1$; a = 4.06 Å, b = 6.66 Å, c = 7.99 Å).[21] This room temperature structure consists of distorted hexagonal close packing (hcp) of sulfur atoms, and three

Received: June 13, 2014
Published: August 18, 2014

   dx.doi.org/10.1021/ja5059185 | J. Am. Chem. Soc. 2014, 136, 12712−12720

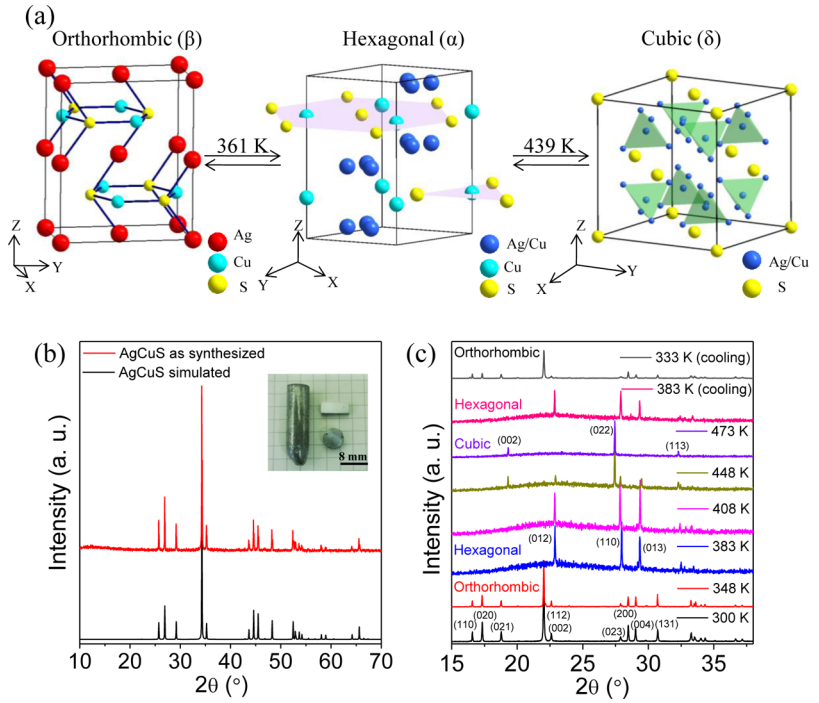

Figure 1. (a) Temperature dependent crystal structural evaluation of AgCuS. In hexagonal phase, Ag and Cu are partially disordered in 12k position. In cubic structure, Ag and Cu are disordered in 8c and 32f positions.[21] (b) Powder XRD pattern measured at lab source (Cu Kα; λ = 1.5406 Å) of room temperature phase of AgCuS with simulated pattern; inset is showing photograph of as-synthesized ingot. Bar- and coin-shaped samples used for transport measurement. (c) Temperature dependent (300−473 K) heating/cooling cycle synchrotron (E = 12.42 keV and λ = 0.998 Å) powder X-ray diffraction patterns of AgCuS.

coordinated Cu atoms that lie in the hcp sulfur layer (Figure 1a). Ag atoms form loosely packed face-centered-cubic (fcc) layers that alternate with those of CuS, and each bonded to two sulfur atoms having a near-linear geometry (Figure 1a).[20] Below 120 K, γ polymorph of AgCuS crystallizes in $Pmc2_1$ space group, which is a slightly distorted form of the room-temperature structure.[20] Two more structural phase transitions have been reported at higher temperatures, at 361 K (β- α) and 439 K (α - δ), respectively. Superionic α and δ phases are reported to crystallize in the hexagonal ($P6_3/mmc$; a = b = 4.1389 Å, c= 7.0817 Å) and the cubic structure ($Fm\bar{3}m$; a = 5.9863 Å), respectively (Figure 1a).[21−23] In the high temperature superionic α phase, sulfur atoms preserve the hcp sublattice, while Ag and Cu atoms are partially disordered (Figure 1a). The second high temperature superionic δ phase is constituted of a rigid fcc lattice of sulfur atoms, in which cations are randomly distributed at tetrahedral and octahedral interstitial sites (Figure 1a).[20]

Herein, we present a temperature tunable reversible $p-n-p$ type conduction switching along with a colossal change in the thermopower (ΔS of ∼1757 μV K^{-1}) at the superionic phase transition (T of ∼364 K) in the crystalline ingot of AgCuS. AgCuS also exhibits ultralow thermal conductivity (0.5−0.7 W/mK) in the temperature range of 300−550 K. Temperature dependent Raman spectroscopy shows a clear variation in Raman spectra during the phase transition temperature and existence of Cu−S bond during ($\beta-\alpha$) phase transition. Our first-principles density functional theoretical calculations reveal the existence of semimetallic intermediate states (constituting of hybridized Cu−S orbital) with Fermi level cutting into the conduction band that overlaps with valence band during the orthorhombic (β) to hexagonal (α) phase transition, which is responsible for the observed $p-n-p$ type conduction switching in AgCuS. We show that electronic states of the rigid sulfur sublattice are primarily responsible for electronic charge transport, whereas phonon spectrum suggests that disordering and soft vibrations of Ag and Cu atoms are responsible for the observed low thermal conductivity. Thus, an effective decoupling of electronic and phonon transport is evident in AgCuS.

EXPERIMENTAL SECTION

Materials. The following elements were purchased from Alfa Aesar and used for the synthesis without further purification. Elemental silver (Ag, 99.999%, metal basis), elemental copper (Cu, 99.9999%, metal basis), and elemental sulfur (S, 99.999%).

Synthesis. Ingot (∼7 g) of AgCuS has been synthesized by mixing appropriate ratios of high-purity starting materials of Ag (3.6938 g, 0.03424 mol), Cu (2.1761 g, 0.03424 mol), and S (1.0978 g, 0.03424 mol) in quartz tube. The tubes were sealed under high vacuum (∼10^{-5} Torr) and slowly heated to 773 K over 12 h, then heated to 1223 K in 5 h, soaked for 24 h, and subsequently air quenched to room temperature. For electrical transport and thermal transport measurements, the sample was cut and polished. In Figure 1, we have shown a photograph of "as synthesized" high quality ingot of AgCuS with bar and coin shaped sample obtained after cutting and polishing the ingot. Bar-shaped sample is used for electrical transport measurement, whereas coin-shaped sample is used for thermal conductivity measurement.

Powder X-ray Diffraction. Room temperature powder X-ray diffraction of the sample was recorded using a Cu Kα (λ = 1.5406 Å) radiation on a Bruker D8 diffractometer. Temperature dependent X-ray diffraction measurements under N_2 flow were carried out with X-ray beam of E = 12.42 keV and λ = 0.998 Å, at BL-18B (Indian beamline), Photon Factory, KEK, Tsukuba, Japan. Energy of the beam was set by Si(111) double crystal monochromator, which was cross checked with Si (640b NIST) standard. All the measurements were carried out in Bragg−Brentano geometry with a divergence slit (300 μm), an antiscattering slit (350 μm), and a receiving slit (300 μm). High temperature measurements were carried out with Anton Paar DHS 1100 heat cell.

dx.doi.org/10.1021/ja5059185 | J. Am. Chem. Soc. 2014, 136, 12712−12720

Differential Scanning Calorimetry. DSC data were measured by Netzsch DSC 200F3 with a heating/cooling rate of 20 K/min between 290 and 550 K in N_2 atmosphere.

Band Gap Measurements. To probe optical energy gap of these compounds, optical diffuse reflectance measurements were performed on finely ground powders at room temperature. The spectra were recorded at the range of 200−3000 nm using a PerkinElmer Lambda 900, UV/vis/NIR spectrometer. Absorption (α/Λ) data were calculated from reflectance data using Kubelka−Munk equations: $\alpha/\Lambda = (1-R)^2/(2R)$, where R is the reflectance and α and Λ are the absorption and scattering coefficients, respectively.

Raman Spectroscopy. Temperature-dependent (300−473 K) Raman spectroscopy measurements were carried out with a LABRAM HR spectrometer. The excitation wavelength of the laser was 514 nm.

Positron Annihilation Spectroscopy. The positron annihilation lifetimes have been measured with a fast−fast coincidence assembly consisting of two constant fraction differential discriminators (Fast ComTech; Model number: 7029A). The detectors are 25 mm-long × 25 mm tapered to 13 mm diameter (truncated conical) BaF_2 scintillators optically coupled to Philips XP2020Q photomultiplier tubes having a time resolution (full width at half-maximum, fwhm) of ∼200 ps. For the present positron annihilation studies, a 10 μCi ^{22}Na source of positrons (enclosed between ∼1.5 μm thin nickel foils) has been sandwiched between two identical samples. A total of 1.5×10^7 coincidence counts have been recorded. Computer program PATFIT-88 has been used along with necessary source corrections to evaluate all the measured positron lifetime spectra. Source component has been evaluated by measuring positron lifetime spectrum of 99.9999% pure Al sample. For the Doppler broadening measurement, a HPGe detector (Efficiency, 12%; Type, PGC 1216sp of DSG, Germany) having energy resolution of 1.15 at 514 keV of ^{85}Sr has been used. To heat the sample, an oven type furnace (30−600 °C with ±2 °C at the sample site) has been attached in the system. For each temperature, about 2×10^7 counts have been recorded in a dual ADC based multiparameter data acquisition system (MPA-3 of FAST ComTec., Germany). The Doppler broadening spectra have been analyzed by evaluating the S-parameter defined by the ratio of the counts in the central area of the 511 keV photopeak (|511 keV − $E\gamma$| ≤ 0.85 keV) and the total area of the photo peak (|511 keV − $E\gamma$| ≤ 4.25 keV).

Seebeck Coefficient and Electrical Conductivity. Seebeck coefficient and electrical conductivity were measured on a sample of the dimension, 2 mm × 3 mm × 8 mm, under helium atmosphere from 290 to 550 K by ULVAC-RIKO ZEM-3 instrument. The longer direction of the sample coincides with the direction in which the thermal conductivity was measured.

Thermal Transport. Thermal diffusivity, D, was directly measured in the range of 290−550 K by laser flash diffusivity method in a Netzsch LFA-457 under N_2 atmosphere. A thin cylinder with 8 mm diameter and 2 mm thickness was used in this measurement. Temperature dependent heat capacity, C_p, was measured in a Netzsch DSC 200F3 differential scanning calorimeter. The total thermal conductivity, κ_{total}, was calculated using the formula, $\kappa_{total} = DC_p\rho$, where ρ is the density of the sample, measured using sample dimension and mass. The density of the pellets obtained was 6.14 g cm^{-3}, which is ∼98% of the theoretical density.

Computational Details. Density functional theory based first-principles calculations of the orthorhombic, hexagonal, and cubic phases of AgCuS were carried out with a general gradient approximation (GGA(PBE))[24] method as implemented in Quantum Espresso package.[25] On-site electron correlations of d-electrons of Ag and Cu atoms, modeled with Hubbard U parameter (5 eV) following earlier work on this material,[20] are tested to give a reasonable band gap of the orthorhombic structure of AgCuS. Plane wave basis was truncated with energy cutoffs of 40 and 480 Ry in representation of wave functions and density, respectively, and 6 × 4 × 3 (orthorhombic), 6 × 6 × 3 (hexagonal), and 4 × 4 × 4 (cubic) k-meshes are used to sample Brillouin zone integration. To model partial (in hexagonal phase) and mixed (in cubic phase) occupancy at Cu and Ag sites, we fix the atomic configuration to maintain the symmetry of the crystal in calculation of electronic structure. To understand the structural stability, we have determined complete phonon dispersion using density-functional perturbation theory (DFPT).[26] To study the orthorhombic to hexagonal phase transition, we have used a 12 atom supercell by considering that the [100] axis of orthorhombic structure transforms to [110] axis of hexagonal structure. Cell parameter of the simulation box is taken to be the average of the experimental cell parameter of the orthorhombic structure and that of the supercell of the hexagonal structure. We have employed Nudged Elastic Band (NEB) based transformation path simulation with 28 intermediate snap shots.[25] NEB is used to search minimum energy pathway and the transition state configuration at the saddle point for a chemical reaction with known initial and final states. To find the minimum energy path, NEB uses a set of images generated by linear interpolation between the given initial and final states. Each "image" corresponds to specific geometry of atoms/ions of the system along this (guessed) reaction path. NEB minimizes energy of such string of images to finally achieve minimum energy path for the reaction.

RESULTS AND DISCUSSION

High quality crystalline ingot of AgCuS (inset of Figure 1b) was prepared by the melting reaction of elemental Ag, Cu and S inside a vacuum sealed quartz tubes. Room temperature powder X-ray diffraction (PXRD) pattern (Figure 1b) measured in in-house X-ray diffractometer (Cu Kα; λ = 1.5406 Å) of the as synthesized samples could be indexed on the room temperature orthorhombic β-AgCuS phase (space group, $Cmc2_1$) with no other impurity phase being observed within the detection limits of powder XRD. In order to understand the structural evolution with temperature, we have performed temperature dependent (300−473 K) heating/cooling cycle synchrotron PXRD of AgCuS and plotted the data in Figure 1c. Temperature dependent PXRD data clearly shows a structural transition from orthorhombic (β) to hexagonal (α) phase around 365 K.[21] With further increase of the temperature, hexagonal (α) phase transforms to a mixture of hexagonal (α) and cubic phases (δ) and then to pure cubic phase (δ) on further heating to 473 K. The phase transformation is reversible in nature as confirmed by the cooling cycle PXRD data (Figure 1c). We have observed a prominent background in the PXRD patterns (2θ = 21−25°) of high temperature hexagonal and cubic phases, but similar background was not present in the case of room temperature orthorhombic phase (Figure 1c).[21] Hexagonal and cubic phases are the high temperature superionic phases, in which Ag/Cu atoms are disordered, resulted in glass-like behavior, which will be discussed in the later part of the paper. Glassy behavior of the cation sublattice at high temperature gives rise to a prominent background in PXRD patterns for the hexagonal and cubic phases. Result obtained in PXRD is consistent with the DSC data (Figure S1, Supporting Information), which also shows two phase transitions ($\beta-\alpha$ and $\alpha-\delta$) above the room temperature. An extra peak with a maximum at ∼408 K is associated with the low-temperature boundary of the two phase hexagonal-cubic region,[21] which is consistent with the temperature dependent PXRD results.

In Figure 2, we show the temperature dependent Raman spectra of AgCuS, which shows a clear variation in Raman spectra during the phase transition temperature, which we will discuss in detail in the later section. The spectroscopically measured band gap of the bulk β-AgCuS is ∼0.9 eV, which is typical of a narrow band gap semiconductor (Figure 3).

Temperature dependent thermopower (S) data of AgCuS has been presented in Figure 4. At room temperature, the sign of thermopower is positive, which indicates p-type conduction in the orthorhombic β-AgCuS phase. The S value of ∼665 μV K^{-1} is

dx.doi.org/10.1021/ja5059185 | J. Am. Chem. Soc. 2014, 136, 12712−12720

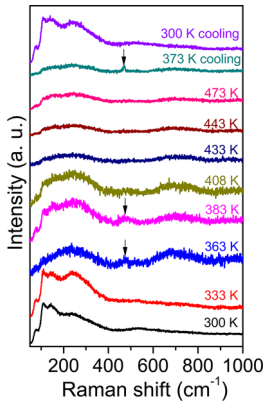

Figure 2. Temperature dependent (300−473) heating/cooling cycle Raman spectra of AgCuS. Black arrow indicates the characteristic Raman peak for Cu−S vibration.

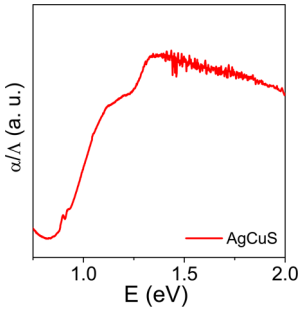

Figure 3. Electronic absorption spectra of β-AgCuS.

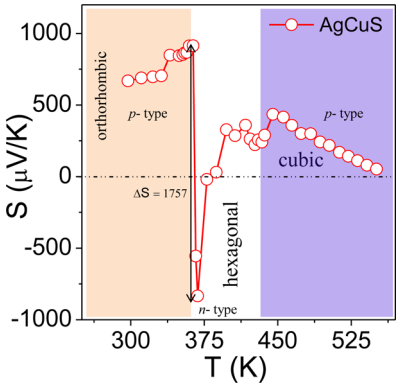

Figure 4. Temperature dependent thermopower of AgCuS.

measured at room temperature, which increases to ~917 μV K^{-1} at 364 K. A colossal change in thermopower (ΔS = 1757 μV K^{-1}) along with a switch from p to n type conduction is observed during orthorhombic to hexagonal ($\beta-\alpha$) superionic phase transition (Figure 4). The thermopower changes from ~917 to about −840 μV K^{-1} at 367 K. Upon further increase in temperature, it reverts back to 30 μV K^{-1} and p-type conduction at 385 K. The $p-n-p$ conduction switching is reversible and reproducible in AgCuS (Figure S2, Supporting Information). The colossal change in the magnitude of thermopower in AgCuS (ΔS = 1757 μV K^{-1}) is indeed sharper and higher than that of $AgBiSe_2$ (ΔS ~730 μV K^{-1}) and $Ag_{10}Te_4Br_3$ (ΔS ~1400 μV K^{-1}).[9,10] More importantly, this property of AgCuS is more readily usable in a device,[7] as the temperature of its transition (T of ~ 360) is closer to room temperature compared to that of $AgBiSe_2$ (T of ~560) and $Ag_{10}Te_4Br_3$ (T of ~380 K). We observe a slight dip in temperature dependent S during the hexagonal to cubic ($\alpha-\delta$) phase transition at 430 K (Figure 4). Temperature dependent electrical conductivity (σ) shows a sharp increase during ($\beta-\alpha$) transition (~364 K), while the increase in σ during ($\alpha-\delta$) transition (~430 K) is not very significant (Figure S3, Supporting Information). Anomalous behavior of temperature dependent σ during ($\beta-\alpha$) transition can be understood by further theoretical calculation of electronic band structure along the transition path, which we will discuss in the later part of the paper.

Figure 5a represents the temperature dependent specific heat (C_p) of AgCuS measured by DSC, which shows two phase transitions above the room temperature. A λ-shaped peak is observed at 380 K (Figure 5a), which corresponds to the orthorhombic to hexagonal phase ($\beta-\alpha$) transition. Such a λ-transition denotes an order−disorder transition, associated with partial disordering of Ag/Cu in the rigid sulfur sublattice during the first superionic phase transition. A broad peak centered at ~430 K (Figure 5a) corresponds to the hexagonal to cubic ($\alpha-\delta$) phase transition. An additional peak with a maximum at ~408 K is associated with the low-temperature boundary of the two phase hexagonal-cubic region,[21] which is consistent with the temperature dependent PXRD results. In the $\beta-\alpha$ phase transition, C_p was dramatically high (λ-transition), while at $\alpha-\delta$ phase transition, C_p shows a broad peak with a low value. Peak centered at ~430 K ($\alpha-\delta$ transition) is broad due to the fact that initially hexagonal (α) phase transforms to a mixture of hexagonal (α) and cubic phases (δ), and then to a pure cubic phase (δ) on increasing the temperature above ~430 K. In the high temperature hexagonal (α) phase, sulfur atoms form the hcp sublattice, while the Ag atoms are fully disordered and Cu atoms are in partially disordered state (Figure 1a). The second high

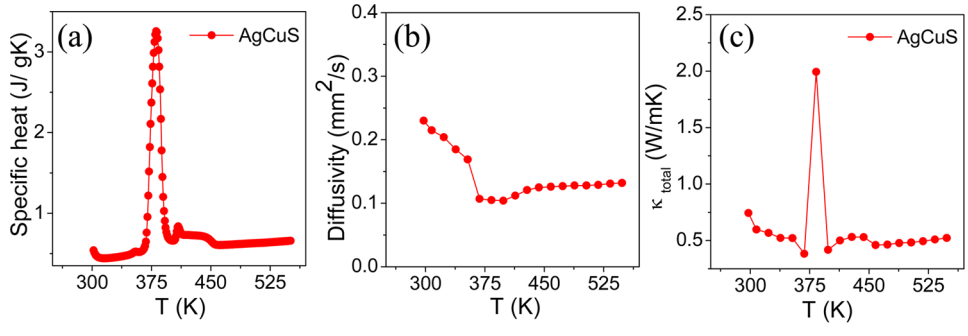

Figure 5. Temperature dependent (a) specific heat, (b) thermal diffusivity, and (c) total thermal conductivity of AgCuS.

dx.doi.org/10.1021/ja5059185 | J. Am. Chem. Soc. 2014, 136, 12712−12720

temperature cubic (δ) phase is constituted of a rigid fcc lattice of sulfur atoms, in which Ag and Cu atoms are completely disordered and distributed at tetrahedral and octahedral interstitial sites (Figure 1a). During first superionic transition ($\beta-\alpha$), the Ag atom gets fully disordered, while 75% Cu atoms reside in ordered position (Figure 1a),[21] resulting in a dramatic change in the temperature dependent C_p due to onset of order−disorder transition. At the second superionic transition ($\alpha-\delta$), Cu atoms gets fully disordered along with the Ag atoms which are already in disordered state in the hexagonal phase (α) and the transition occurs from a partially disordered (existing disordered) state (α) to fully disordered state (δ), giving rise to less dramatic change in C_p compared to the ($\beta-\alpha$) transition. The ($\beta-\alpha$) transition occurs from a ordered state to a partially disordered state with a drastic volume change of 2.3%, while the ($\alpha-\delta$) transition occurs from a partially disordered state to fully disordered state with a volume change of 0.6%.[21] The above discussion suffices as explanation as to why the anomalies in the different measurements (thermopower and C_p) are generally dramatic and sharp during the ($\beta-\alpha$) transition compared to those of ($\alpha-\delta$) transition.

In addition to the spectacular change in thermopower with a conduction switching, AgCuS exhibits low thermal diffusivity and thermal conductivity in 300−550 K temperature range, which is important to maintaining temperature gradients in devices. Temperature dependent total thermal conductivity, κ_{total}, displayed in Figure 5c, was estimated using the formula $\kappa_{total} = DC_p\rho$, where D is the thermal diffusivity (Figure 5b), C_p is the specific heat, and ρ is the density of the sample. We have observed a sharp decrease in the temperature dependent diffusivity at orthorhombic (β) to hexagonal (α) phase transition around 368 K, while during hexagonal (α) to cubic (δ) transition, no significant anomaly has been observed (see Figure 5b). At room temperature, the measured value of κ_{total} is ∼0.7 W m^{-1} K^{-1}. With an increase in temperature, a pronounced peak in κ_{total} (∼1.98 W m^{-1} K^{-1}) is observed at ∼384 K, which is due to the abrupt change in the C_p during the $\beta-\alpha$ phase transition and κ_{total} of ∼0.50 W m^{-1} K^{-1} is measured just after the transition. We observe a decrease in the thermal conductivity from ∼0.53 W m^{-1} K^{-1} to ∼0.45 W m^{-1} K^{-1} during ($\alpha-\delta$) phase transition, which then increases to a value of ∼0.52 W m^{-1} K^{-1} at 550 K. As electrical conductivity of the undoped pristine AgCuS is rather low (Figure S3, Supporting Information), the lattice thermal conductivity ($\kappa_{lattice} = \kappa_{total} - L\sigma T$, where σ is electrical conductivity and L is the Lorentz number) is essentially the same as κ_{total} in AgCuS. Low thermal conductivity over a broad temperature range is achieved in AgCuS, which is possibly due to effective scattering of phonons by the loosely bound and mobile Cu and Ag ions in the rigid sulfur sublattice.

Temperature dependent Raman spectroscopy is a well-known technique to understand the structural change during phase transition. Room temperature Raman spectrum of orthorhombic (β) AgCuS shows a broad peak around 240 cm^{-1}, which is assigned to Ag−S bond vibration.[27,28] Other low energy peaks below 150 cm^{-1} are due to the lattice vibration of Ag/Cu,[29] which is later indicated by detailed phonon dispersion calculations. With increasing the temperature to the ($\beta-\alpha$) transition temperature (363 K), peaks associated with Ag lattice vibration completely disappear as the Ag atoms begin to disorder in the hexagonal (α) phase. At ($\beta-\alpha$) transition temperature (363 K), interestingly a peak appears at 474 cm^{-1}, which is assigned to Cu−S bond vibration.[28] This results indicate that at the *p-n-p* type conduction switching temperature (363 K), Cu−S bonds remain intact, where as Ag atoms become disordered. We will show later through electronic band structure calculation that hybridized Cu−S orbital contributes to the semimetallic intermediate state during ($\beta-\alpha$) phase transition, which is responsible for *p−n−p* type conduction switching in AgCuS. In the hexagonal phase (α), 75% of Cu atoms are ordered, which form the Cu−S bond, whereas the remaining (25%) Cu atoms are in disordered state along with Ag. With further increasing the temperature to 383 K (just above the phase transition), a broad Raman band centered at 240 cm^{-1} reappears which was present in the room temperature orthorhombic (β), indicating the reappearance of weak Ag−S interaction. When AgCuS completely transforms into cubic (δ) phase, Ag/Cu are in fully disordered state, so the macroscopic polarizibility disappears, and no Raman peaks are observed. Similar observation has been reported for $AgBiSe_2$ nanocrystals.[9] In the present case, the phase transition is reversible, which is confirmed by taking the Raman spectra on cooling cycle (see Figure 2).

To understand the origin of the conduction type in orthorhombic β-AgCuS at room temperature, we have performed positron annihilation spectroscopy of AgCuS. The lifetime of the positron determines the type and relative concentration of defects/vacancies.[9,30] Fitting of positron annihilation spectrum (see Figure 6a) at room temperature yields three lifetime values, 154 ± 2 ps with (24 ± 1)% intensity, 272 ± 1 ps with (70 ± 1)% intensity and a very long component of 1568 ± 200 ps with (6 ± 0.2)% intensity. The shortest lifetime component is the free annihilation of positron,[31] while the intermediate component is due to positron annihilation at the defect site which is here the Ag vacancy.[9,31] The long lifetime

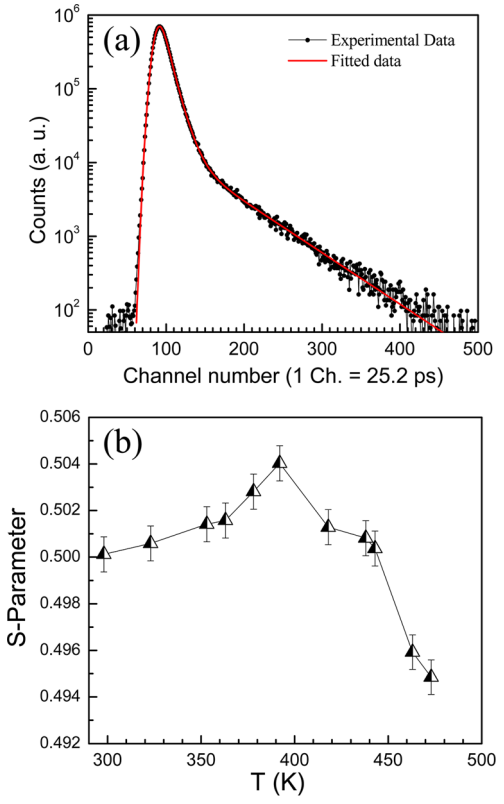

Figure 6. (a) The positron annihilation lifetime spectrum for the AgCuS sample at room temperature. Solid red line shows the fitting for the determination of positron lifetime components. (b) Temperature dependent Doppler broadening *S*-parameter of AgCuS.

dx.doi.org/10.1021/ja5059185 | J. Am. Chem. Soc. 2014, 136, 12712−12720

component originates from the formation of positronium at the sample surface or at the large voids inside the sample.[31] Moreover, density functional theoretical calculation also confirms that the formation energy of Ag vacancy is lowest among the other possible defects in AgCuS sample (Table S1, Supporting Information). These results clearly indicate that the Ag vacancy is indeed responsible for *p*-type conduction in *β*-AgCuS at room temperature and Ag vacancy can possibly acts as effective path for the movement of Ag atoms in the high temperature superionic phases.

Temperature dependent Doppler broadening of the annihilation radiation reflects the momentum distribution of annihilating electrons, which has provided further evidence of *p*−*n*−*p* type conduction switching in AgCuS during (*β*−*α*) transition. The Doppler broadening spectra have been analyzed by evaluating the *S*-parameter defined by the ratio of the counts in the central area of the annihilation photopeak and the total area of the photopeak. Figure 6b represents the temperature dependent Doppler broadening *S*-parameter for AgCuS. The *S*-parameter represents the ratio between the positrons annihilation with lower momentum electrons with the higher momentum electrons. During orthorhombic (*β*) to hexagonal (*α*) phase transformation, onset of *S*-parameter starts at ∼360 K and it reaches a maximum at ∼385 K, indicating most abundant valence electrons (majority carrier for *n*-type conduction), which is also consistent with the electronic band structure calculations discussed in later section. After passing the maximum at 385 K, *S*-parameter decreases, indicating the conduction type changes back to *p*-type. *S*-parameter falls sharply after passing the (*α*−*δ*) phase transition temperature (∼440 K). Similar type behavior in temperature dependent *S*-parameter has been observed in the $AgBiSe_2$ nanocrystals.[9]

To further understand the origin of the significant change in the thermopower with *p*−*n*−*p* type conduction switching and low thermal conductivity, we determine electronic and phonon spectra of AgCuS from first-principles. Phonon dispersion of the orthorhombic *β*-AgCuS phase exhibits a gap that separates high energy modes originating from sulfur sublattice and low energy modes largely involving the Ag/Cu sublattices (Figure 7). This stems from the large mass contrast between the cations and anion in AgCuS. A large number of phonon modes have frequencies below 50 cm^{-1}, which are expected to be strongly influenced by anharmonicity and be sensitive to variation in temperature or the other fields. Three of the calculated phonon modes (at M1, S and M3 point) of *β*-AgCuS have weakly imaginary frequencies in the acoustic branch. M1 mode involves a shear type deformation in the xy direction indicating a cell distortion occurring at low temperature (Figure S4, Supporting Information). The instability (S) is related to Ag atoms, which indicates restricted shear or "flow" in *y*-direction (Figure S4, Supporting Information). The third instability (M3) is a transverse acoustic mode with displacements along *y*-direction (Figure S4, Supporting Information). These instabilities are rather weak and do not quite lower the energy of the structure (as has been verified through explicit simulations of energetics of distortions given by these modes), but suggest a shallow/flat energy landscape.

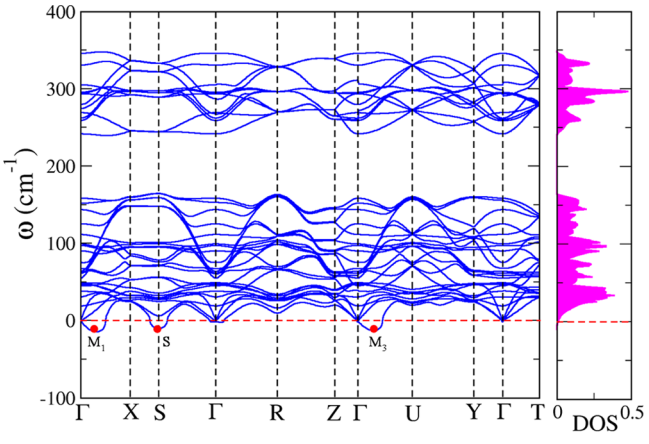

Figure 7. Phonon dispersion plot and phonon density of state of orthorhombic *β*-AgCuS.

The presence of a large number of low energy phonon modes and those related to shear deformation indicate that AgCuS is a soft material, and should possess low thermal conductivity (which depends on square of group velocity of these modes). At higher temperatures, dynamics and renormalization of these cationic low energy phonon modes are relevant ("restricted shear") to the phase transformation and structural disorder observed experimentally. These low frequency shear modes will soften further at higher temperature, and lead to flow of cations or liquid-like behavior. While sulfur atoms form a rigid high symmetry hexagonal lattice with void spaces, Ag/Cu atoms are relatively free to move by hopping between the vacant sites within the sulfur sublattice. A similar phenomenon has been studied in superionic Cu_2Se and Cu_2S with rigid anion and liquid-like cation lattices.[3,32,33] Such liquid-like behavior of the sublattice of heavy cations leads to effective phonon scattering, thereby reducing thermal conductivity in AgCuS.

In Figure 8, we show electronic structure and partial density of states (PDOS) of the observed phases of AgCuS. Theoretical estimate of the band gap of the orthorhombic *β*-AgCuS phase is ∼0.92 eV (Figure 8a), close to the observed value. The degeneracy between valence band maxima at Z and Γ points in *β*-AgCuS allows coexistence of holes in two distinct valleys (pockets) leading to a high *p*-type thermopower. Analysis of the PDOS shows that the electronic states in the 2 eV window of valence band maximum are constituted solely of sulfur *p* orbitals (Figure 8b). Interestingly, in this energy window, p_x and p_y orbitals of sulfur create the frontier states, whereas p_z orbitals are slightly lower in energy (∼1 eV lower than E_F), as clearly evident in Figure 8b. A strong covalency within the planar framework of sulfur and copper ions is essentially responsible for the electronic conduction. Orbitals of Ag atoms are positioned much deeper in energy, and are unlikely to contribute to the electronic conduction.

Electronic structure of the hexagonal phase shows a narrow band gap of ∼0.14 eV (Figure 8c), with a strong electron hole asymmetry responsible for its high thermopower. Hole carriers have much higher effective mass (m_h*) than that of electron carriers (m_e*) (Figure 8c). The structure of sulfur sublattice involves a chain-like formation along the *z*-direction, and its signature is evident in the PDOS (Figure 8d), where p_z orbitals of sulfur constitute the valence states within 1 eV below E_F. The states at the valence band maximum at (0,0,0.6) are responsible for electrical conduction by holes along the chains of sulfur atoms. Quantum confinement of holes in the hexagonal sulfur sublattice along one dimension (*z*) leads to a high effective mass of valence band (flat band) and a large Seebeck coefficient.

The switching associated with *p*−*n*−*p* type conduction during the orthorhombic to hexagonal phase (*β*−*α*) transition can be understood from the electronic structure of AgCuS along the transition path, which we determine using a nudged elastic band

dx.doi.org/10.1021/ja5059185 | J. Am. Chem. Soc. 2014, 136, 12712−12720

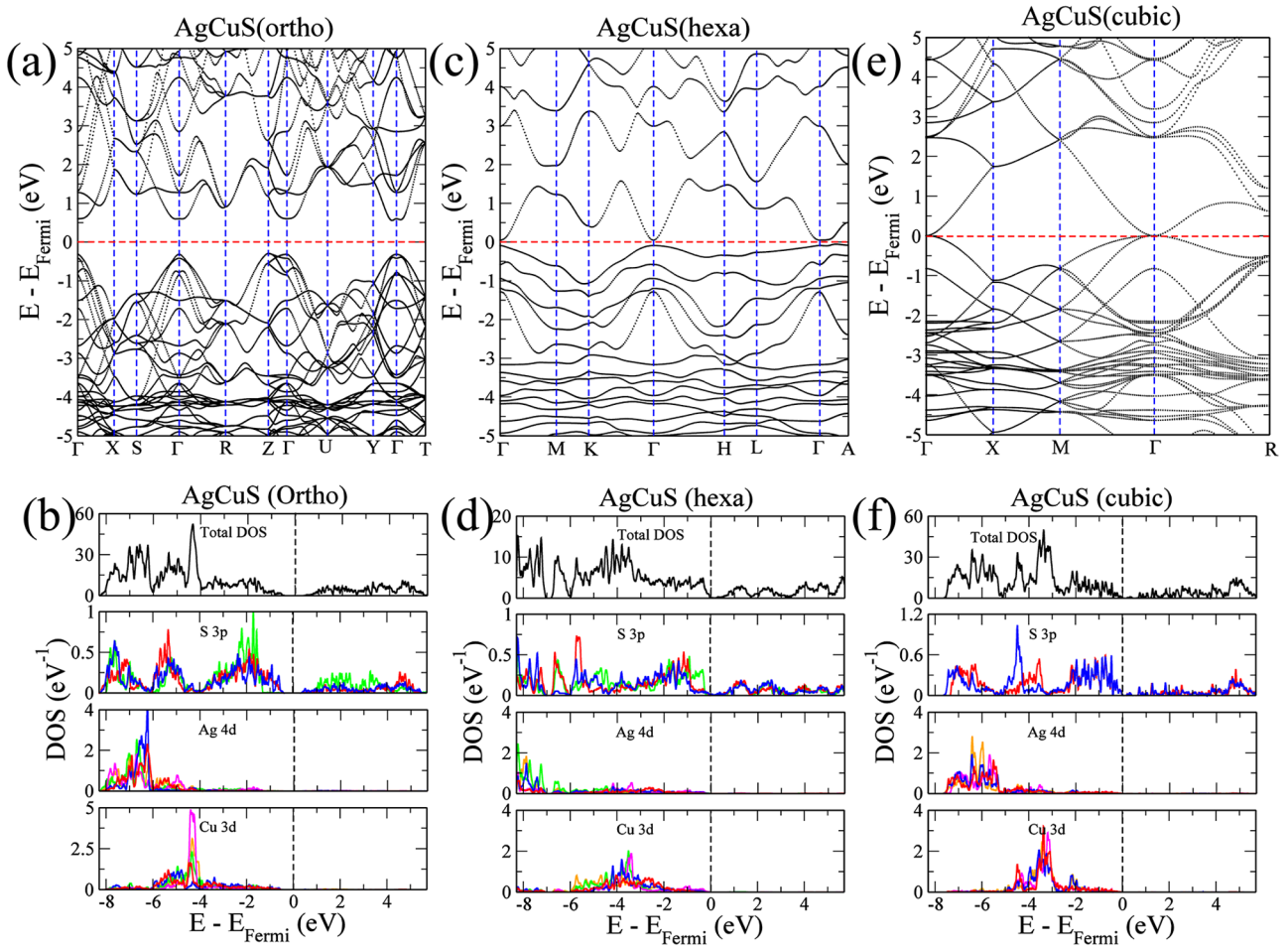

Figure 8. Electronic band structure and density of state (total and atom projected) of (a and b) orthorohmbic, (c and d) hexagonal, and (e and f) cubic phase of AgCuS. (Color code) S 3p orbitals: red line is p_x, blue line is p_y and, green line is p_z. Ag 4d and Cu 3d orbitals: red line is d_{xy}, magenta line is d_{yz}, green line is d_{zx}, orange line is d_{z^2} and blue line is $d_{x^2-y^2}$.

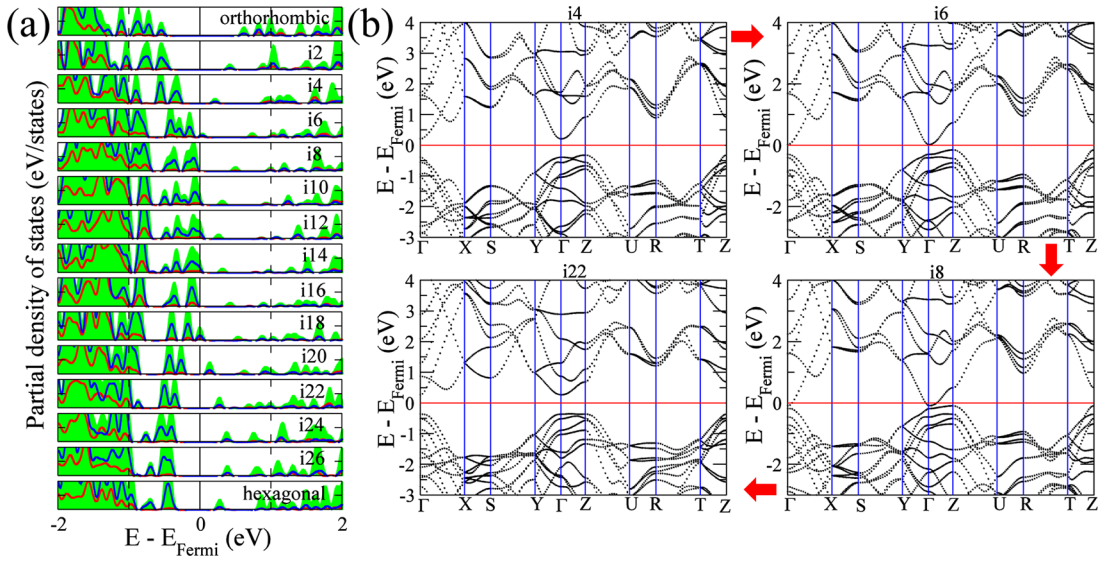

Figure 9. (a) Partial density of states of AgCuS along the minimum energy path of orthorhombic to hexagonal phase transformation as predicted by NEB calculation. Green, red, and blue colors in (a) represent partial density of states of S 3p, Ag 4d, and Cu 3d, respectively. (b) Electronic band structures of intermediate (i) states during orthorhombic to hexagonal phase transformation.

technique.[25] The energy barrier of this transformation is 0.6 eV. Evolution of partial density of states along the transition path shows existence of semimetallic intermediate states (i10, i12, i14 and i18) near the energy barrier or the transition state of the phase transformation (Figure 9a). Due to atomic movement involved in disordering of the cationic sublattices, there are

dx.doi.org/10.1021/ja5059185 | J. Am. Chem. Soc. 2014, 136, 12712−12720

changes in bonding reflected in mixing between the states in valence and conduction bands. This results in downward and upward shifts in the conduction and valence bands, respectively (see Figure 9a and video in the Supporting Information), and in overlapping valence and conduction bands in a small energy interval near the gap, and hence the semimetallic state. Electronic structure of the intermediate states (Figure 9b) clearly shows that the Fermi level first initially moves into the conduction band (i6 and i8, Figure 9b), and a gap opens up again with a shift (i22, Figure 9b) of the conduction band to higher energy, as the transition proceeds from orthorhombic to hexagonal phase. The *n*-type carriers of the intermediate semimetallic state are responsible for the *p*−*n*−*p* type conduction switching during (*β*−*α*) transition. Unlike the orthorhombic or hexagonal phases where the states near Fermi energy are dominated by sulfur orbitals, contribution from hybridized Cu−S orbitals to the overlapping valence and conduction band gives rise to semimetallic character (and *n*-type conduction) of the intermediate structure. While the existence of a semimetallic intermediate state was suggested to be responsible for the *p*−*n*−*p* conduction switching reported earlier in $AgBiSe_2$ nanocrystals[9] and $Ag_{10}Te_4Br_3$,[10] our work establishes this unambiguously in AgCuS. Existence of semimetallic states during the (*β*−*α*) transition resulted in sharp increase in the temperature dependent electrical conductivity at 364 K (Figure S3, Supporting Information). Finally, our calculated electronic structure of the cubic *δ*-AgCuS (Figure 8e) clearly shows a vanishing band gap. The disorder in cation sublattices and anharmonicity of the associated soft modes lead to strong phonon scattering, and hence an ultralow thermal conductivity of the cubic phase.

CONCLUSIONS

In conclusion, temperature tunable *p*−*n*−*p* conduction switching with a colossal change in thermopower has been achieved in a single compound, AgCuS, which is free of expensive and less abundant Se/Te. Temperature dependent synchrotron powder X-ray diffraction, heat capacity, positron annihilation spectroscopy and Raman spectroscopy of AgCuS clearly explain the phase transition behavior and provide fundamental insight into the *p*−*n*−*p* type conduction switching. Ag vacancy is responsible for *p*-type conduction in *β*-AgCuS at room temperature and acts as effective path for the movement of Ag atoms during (*β*−*α*) phase transition, whereas Cu−S bonds remain intact. An intermediate semimetallic state, constituting of hybridized Cu−S orbitals, arises from reshuffling of electronic orbitals contributing to valence and conduction bands during the orthorhombic to hexagonal phase transition, which is responsible for the *p*−*n*−*p* conduction switching in AgCuS. Temperature dependent Doppler broadening of positron annihilation indicates that semimetallic intermediate state contributes more conduction electron during (*β*−*α*) transition, which essentially leads to *p*−*n*−*p* type conduction switching. Electronic density of states and phonon dispersion reveal that the rigid sulfur sublattice is primarily responsible for the electronic charge transport, whereas soft vibrations and mobility of Ag/Cu ions are responsible for the ultralow thermal conductivity. Such decoupling of electronic and phonon transport leads to a unique combination of temperature dependent *p*−*n*−*p* conduction switching and ultralow thermal conductivity in AgCuS near room temperature, opening up a new class of temperature controlled diode or transistor devices based on a single compound.

ASSOCIATED CONTENT

Supporting Information

Additional data, DSC plot of AgCuS, thermopower of different samples of AgCuS, temperature dependent electrical conductivity of AgCuS, imaginary phonon modes in orthorhombic AgCuS, table of the formation energy of a defect in the *β*-AgCuS, and video of downward and upward shifts of the conduction and valence bands during (*β*-*α*) transition. This material is available free of charge via the Internet at http://pubs.acs.org.

AUTHOR INFORMATION

Corresponding Author

kanishka@jncasr.ac.in

Notes

The authors declare no competing financial interest.

ACKNOWLEDGMENTS

This work was supported by DST Ramanujan Fellowship, New Chemistry Unit and Sheikh Saqr Laboratory. S.N.G thanks JNCASR for a research fellowship. U.V.W acknowledges support from a J. C. Bose National Fellowship. Authors thank the Department of Science and Technology, India, for the financial support and Saha Institute of Nuclear Physics, India, for facilitating the experiments at the Indian Beamline, Photon Factory, KEK, Japan. Authors also thank Dr. Velaga Srihari for maintaining the beamline during XRD data collection.

REFERENCES

(1) Rao, C. N. R. *Acc. Chem. Res.* **1984**, *17*, 83.
(2) Coronado, E.; Marti-Gastaldo, C.; Navarro-Moratalla, E.; Ribera, A.; Blundell, S. J.; Baker, P. J. *Nat. Chem.* **2010**, *2*, 1031.
(3) Liu, H.; Shi, X.; Xu, F.; Zhang, L.; Zhang, W.; Chen, L.; Li, Q.; Uher, C.; Day, T.; Snyder, G. J. *Nat. Mater.* **2012**, *11*, 422.
(4) Keen, D. A. *J. Phys.: Condens. Matter* **2002**, *14*, R819.
(5) Ohkoshi, S.-I.; Tsunobuchi, Y.; Matsuda, T.; Hashimoto, K.; Namai, A.; Hakoe, F.; Tokoro, H. *Nat. Chem.* **2010**, *2*, 539.
(6) Liu, J.; Gottschall, T.; Skokov, K. P.; Moore, J. D.; Gutfleisch, O. G. *Nat. Mater.* **2012**, *11*, 620.
(7) Janek, J. *Nat. Mater.* **2009**, *8*, 88.
(8) Lange, S.; Nilges, T. *Chem. Mater.* **2006**, *18*, 2538.
(9) Xiao, C.; Qin, X.; Zhang, J.; An, R.; Xu, J.; Li, K.; Cao, B.; Yang, J.; Ye, B.; Xie, Y. *J. Am. Chem. Soc.* **2012**, *134*, 18460.
(10) Nilges, T.; Lange, S.; Bawohl, M.; Deckwart, J.-M.; Janssen, M.; Wiemhöfer, H.-D.; Decourt, R.; Chevalier, B.; Vannahme, J.; Eckert, H.; Weihrich, R. *Nat. Mater.* **2009**, *8*, 101.
(11) Terabe, K.; Hasegawa, T.; Nakayama, T.; Aono, M. *Nature* **2005**, *433*, 47.
(12) Waser, R.; Aono, M. *Nat. Mater.* **2007**, *6*, 833.
(13) Biswas, K.; He, J.; Blum, I. D.; Wu, C. I.; Hogan, T. P.; Seidman, D. N.; Dravid, V. P.; Kanatzidis, M. G. *Nature* **2012**, *489*, 414.
(14) Zhao, L.-D.; Lo, S.-H.; Zhang, Y.; Sun, H.; Tan, G.; Uher, C.; Wolverton, C.; Dravid, V. P.; Kanatzidis, M. G. *Nature* **2014**, *508*, 373.
(15) Miller, T. A.; Wittenberg, J. S.; Wen, H.; Connor, S.; Cui, Y.; Lindenberg, A. M. *Nat. Commun.* **2013**, *4*, 1369.
(16) Nilges, T.; Nilges, S.; Pfitzner, A. *Chem. Mater.* **2004**, *16*, 806.
(17) Osters, O.; Bawohl, M.; Bobet, J. L.; Chevalier, B.; Decourt, R.; Nilges, T. *Solid State Sci.* **2011**, *13*, 944.
(18) Ishiwata, S.; Shiomi, Y.; Lee, J. S.; Bahramy, M. S.; Suzuki, T.; Uchida, M.; Arita, R.; Taguchi, Y.; Tokura, Y. *Nat. Mater.* **2013**, *12*, 512.
(19) Maier, J. *Nat. Mater.* **2005**, *4*, 805.
(20) Perez, S. D.; Garcia, M. A.; Garcia, M. D.; Domene, G. B.; Mühle, C.; Jansen, M. *Inorg. Chem.* **2013**, *52*, 355.
(21) Trots, D. M.; Skomorokhov, A. N.; Knapp, M.; Fuess, H. *J. Phys.: Condens. Matter* **2007**, *19*, 136204.
(22) Djurle, S. *Acta Chem. Scand.* **1958**, *12*, 1427.

(23) Skinner, B. *J. Econ. Geol.* **1966**, *61*, 1.
(24) Perdew, J. P.; Burke, K.; Ernzerhof, M. *Phys. Rev. Lett.* **1996**, *77*, 3865.
(25) Giannozzi, P.; Baroni, S.; Bonini, N.; Calandra, M.; Car, R.; Cavazzoni, C.; Ceresoli, D.; Chiarotti, G. L.; Cococcioni, M.; Dabo, I.; Corso, A. D.; Gironcoli, S. de.; Fabris, S.; Fratesi, G.; Gebauer, R.; Gerstmann, U.; Gougoussis, C.; Kokalj, A.; Lazzeri, M.; Martin-Samos, L.; Marzari, N.; Mauri, F.; Mazzarello, R.; Paolini, S.; Pasquarello, A.; Paulatto, L.; Sbraccia, C.; Scandolo, S.; Sclauzero, G.; Seitsonen, Ari P.; Smogunov, A.; Umari, P.; Wentzcovitch, R. M. *J. Phys.: Condens. Matter* **2009**, *21*, 395502.
(26) Baroni, S.; de Gironcoli, S.; Dal Corso, A. *Rev. Mod. Phys.* **2001**, *73.2*, 515.
(27) Milekhin, A.; Sveshnikova, L.; Duda, T.; Surovtsev, N.; Adichtchev, S.; Zahn, D. R. T. *Chin. J. Phys.* **2011**, *49*, 63.
(28) Sukarova, M. B.; Najdoski, M.; Grozdanov, M.; Chunnilall, C. J. *J. Mol. Struct.* **1977**, *410*−*411*, 267.
(29) Ishii, M.; Wada, H. *Mater. Res. Bull.* **1993**, *28*, 1269.
(30) Sarkar, A.; Chakrabarti, M.; Ray, S. K.; Bhowmic, D.; Sanyal, D. *J. Phys.: Condens. Matter* **2011**, *23*, 155801.
(31) Krause-Rehberg, R.; Leipner, H. S. *Positron Annihilation in Semiconductors*; Springer Verlag: Berlin, 1999.
(32) He, Y.; Day, T.; Zhang, T.; Liu, H.; Shi, X.; Chen, L.; Snyder, G. J. *Adv. Mater.* **2014**, *26*, 3974.
(33) Wang, L.-W. *Phys. Rev. Lett.* **2012**, *108*, 085703.